AIChE

Partial Oxidation of Palm Fatty Acids Over Ce-ZrO_2: Roles of Catalyst Surface Area, Lattice Oxygen Capacity and Mobility

Navadol Laosiripojana
The Joint Graduate School of Energy and Environment, CHE Center for Energy Technology and Environment, King Mongkut's University of Technology Thonburi, Bangkok 10140, Thailand

Worapon Kiatkittipong
Dept. of Chemical Engineering, Faculty of Engineering and Industrial Technology, Silpakorn University, Nakhon Pathom 73000, Thailand

Suttichai Assabumrungrat
Dept. of Chemical Engineering, Faculty of Engineering, Chulalongkorn University, Bangkok 10330, Thailand

DOI 10.1002/aic.12491
Published online December 29, 2010 in Wiley Online Library (wileyonlinelibrary.com).

Nanoscale Ce-ZrO_2, synthesized by cationic surfactant-assisted method, has useful partial oxidation activity to convert palm fatty acid distillate (PFAD; containing C_{16}–C_{18} compounds) to hydrogen-rich gas with low carbon formation problem under moderate temperatures. At 1123 K with the inlet O/C ratio of 1.0, the main products from the reaction are H_2, CO, CO_2, and CH_4 with slight formations of gaseous high hydrocarbons (i.e., C_2H_4, C_2H_6, and C_3H_6), which could all be eliminated by applying higher O/C ratio (above 1.25) or higher temperature (1173 K). Compared with the microscale Ce-ZrO_2 synthesized by conventional coprecipitation method, less H_2 production with relatively higher C_2H_4, C_2H_6, and C_3H_6 formations are generated from the reaction over microscale Ce-ZrO_2. The better reaction performances of nanoscale Ce-ZrO_2 are linearly correlated with its higher specific surface area as well as higher oxygen storage capacity and lattice oxygen mobility, according to the reduction/oxidation measurement and $^{18}O/^{16}O$ isotope exchange study. © 2010 American Institute of Chemical Engineers *AIChE J*, 57: 2861–2869, 2011

Keywords: palm fatty acid distillate, hydrogen, partial oxidation, reforming, Ce-ZrO_2

Introduction

Hydrogen-rich gas is the major fuel for solid oxide fuel cell, which can be readily produced from the reactions of several hydrocarbons, i.e., methane, methanol, ethanol, liquefied petroleum gas, gasoline, and other oil derivatives with oxygen-containing coreactants, i.e., O_2, H_2O, and CO_2. Partial oxidation, steam reforming, and the combination of both reactions (as called autothermal reforming) have been known as feasible processes to produce hydrogen-rich fuel from several hydrocarbons.[1,2] Steam reforming is currently the most common process for producing hydrogen[1]; however, it has a disadvantage of slow startup, which makes it more suitable for a stationary system rather than for a mobile system.[2] Recently, catalytic partial oxidation[3–6] and autothermal reforming[7,8] appear to have attracted much interest. The partial oxidation consists of substoichiometric oxidation of hydrocarbons, whereas the autothermal reforming integrates

Correspondence concerning this article should be addressed to N. Laosiripojana at navadol_l@jgsee.kmutt.ac.th.

partial oxidation with steam reforming. Theoretically, both partial oxidation and autothermal reforming offer significant lower energy requirement and higher gas-space velocity than steam reforming reaction.[9]

Focusing on fuel selection, because of the current oil crisis and shortage of fossil fuels, the development of H_2 production process from biomass-based feedstock attracts much attention. Among them, palm oil is one of the current attractive feedstocks that has widely been converted to transportation fuel (e.g., biodiesel via transesterification process). Generally, crude palm oil (CPO) always contains high amount of free fatty acid (FFA), and the presence of too high FFA could easily result in high amounts of soap produced during the transesterification reaction. To avoid this reaction, FFA must be initially removed from CPO (as called palm fatty acid distillate or PFAD). The conversion of this PFAD to valuable products, e.g., hydrogen-rich gas would provide the great benefit in terms of energy and environmental aspects as well as reducing the cost of biodiesel production, enabling biodiesel to compete economically with conventional petroleum diesel fuels. Practically, PFAD consists mainly of palmitic acid ($C_{16}H_{32}O_2$: $CH_3(CH_2)_{14}COOH$), oleic acid ($C_{18}H_{34}O_2$: $CH_3(CH_2)_7CH{=}CH(CH_2)_7COOH$), and linoleic acid ($C_{18}H_{32}O_2$: $CH_3(CH_2)_4CH{=}CHCH_2CH{=}CH(CH_2)_7CO_2H$) with various ratios depending on the source of oils. These high hydrocarbon compounds should be efficiently used as the feedstock for H_2 production. Nevertheless, until now, only a few works have presented the catalytic reforming or cracking of acetic acid and/or heavy hydrocarbons to H_2.[10-12] Theoretically, the major difficulty to reform the heavy hydrocarbon compounds like PFAD is the possible degradation of catalyst due to the carbon deposition as PFAD can homogenously decompose to several gaseous hydrocarbon elements, which could further decompose to carbon species and deposit on the surface of catalyst.

In this work, Ce-ZrO_2 was applied as oxidative catalyst because ceria-based materials were known as an alternative reforming catalyst, which can reform hydrocarbons and oxyhydrocarbons efficiently with high resistance toward carbon formation because of their high oxygen storage capacity (OSC) and redox property.[13–19] The addition of zirconium oxide (ZrO_2) to ceria has also been known to improve the specific surface area, the OSC, the redox property, the thermal stability and the catalytic activity of ceria.[20–26] In this study, Ce-ZrO_2 was mainly prepared by cationic surfactant-assisted method because we previously reported the achievement of nanoscale material with high surface area and good stability from this preparation technique, which is mainly due to the interaction of hydrous oxide with cationic surfactants under basic condition.[27,28] It is noted that the performances of Ce-ZrO_2 prepared by this method in terms of partial oxidation activity, resistance toward carbon formation, and the redox properties (i.e., OSC and lattice oxygen mobility) were also compared with those of Ce-ZrO_2 synthesized by the typical coprecipitation method.

Experimental

Raw material

PFAD was obtained from Chumporn Palm Oil Industry Public Company, Thailand. It consists of 93 wt % FFA (mainly contains 46% palmitic acid, 34% oleic acid, and 8% linoleic acid with small amount of other fatty acids, i.e., stearic, myristic, tetracosenoic, linolenic, ecosanoic, ecosenoic, and palmitoleic acid). The rest of the elements are triglycerides, diglycerides, monoglycerides, and traces of impurities.

Catalyst preparation and characterization

Ce-ZrO_2 was chosen as an oxidative catalyst in this work. The materials with different Ce/Zr molar ratios were prepared by coprecipitation of cerium nitrate ($Ce(NO_3)_3{\cdot}H_2O$) and zirconium oxychloride ($ZrOCl_2{\cdot}H_2O$) (from Aldrich) in the presence of 0.1 M cetyltrimethylammonium bromide solution (from Aldrich) as a cationic surfactant. The ratio between both solutions was altered to achieve Ce/Zr molar ratios of 1/3, 1/1, and 3/1, whereas the molar ratio of (([Ce]+[Zr])/[cetyltrimethylammonium bromide] was kept constant at 0.8. The solid solution was formed by the slow mixing of this metal salt solution with 0.4 M urea. After preparation, the precipitate was filtered and washed with deionized water and ethanol to prevent an agglomeration of the particles. It was dried overnight in an oven at 383 K and then calcined in air at 1173 K for 6 h. According to the preparation of Ce-ZrO_2 by coprecipitation method, similar procedure as described above without adding of cetyltrimethylammonium bromide solution was applied. From the preparations, high specific surface area Ce-ZrO_2 (with the specific surface area of 46.5, 47, and 49 $m^2\ g^{-1}$ for the catalysts with Ce/Zr of 3/1, 1/1, and 1/3, respectively) and average particle size of 50–80 nm (less than 100 nm; so-called nanoscale Ce-ZrO_2) can be achieved from the surfactant-assisted method, whereas relatively lower specific surface area (20, 20.5, and 22 $m^2\ g^{-1}$ for the catalysts with Ce/Zr of 3/1, 1/1, and 1/3, respectively) with average particle size of 100–150 μm was obtained from the coprecipitation method. It is noted that the average catalyst particle sizes were estimated by the nanosizer and the particle size analyzer. To investigate the OSC and lattice oxygen mobility of synthesized catalysts, the reduction/oxidation measurement and $^{18}O/^{16}O$ isotope exchange study were applied; details of these studies are described in Section "reactivity of Ce-ZrO_2 toward partial oxidation of PFAD."

It is noted that, for comparison, Ni/Ce-ZrO_2 (with 5 wt % Ni) was also tested for steam reforming reaction in this work. They were prepared by impregnating Ce-ZrO_2 with $Ni(NO_3)_2$ solution (from Aldrich). The catalysts were calcined at 1173 K and reduced under H_2 flow at 573 K for 6 h before use. After treatment, the catalysts were characterized by several physicochemical methods, i.e., the weight contents of Ni were determined by X-ray fluorescence analysis; the reducibility of catalyst was calculated from the degree of H_2 uptakes from the temperature-programed reduction testing; the dispersion percentage was identified from the volumetric H_2 chemisorption measurement using chemisorption analyzer; and the catalyst specific surface area was obtained from BET measurement. According to these characterizations, the catalyst consists of 5.01% Ni loading content with the reducibility and Ni dispersion of 92.6 and 8.95%, respectively. Furthermore, the specific surface area was observed to be 41.5 $m^2\ g^{-1}$.

Apparatus and procedures

An experimental system was designed and constructed as shown elsewhere.[27] The feed gases, i.e., He (as carrier gas), O_2 and H_2 (used to reduce Ni/Ce-ZrO_2) were controlled by three mass flow controllers, whereas PFAD and water were introduced by the heated syringe pump (with the reactant feed flow rate of 2.54 $cm^3\ h^{-1}$) and vaporized by our designed quartz vaporizer-mixer system. These gaseous feed was introduced to the 10-mm-diameter quartz reactor, which was mounted vertically inside a tubular furnace. A Type-K thermocouple was placed into the annular space between the reactor and furnace. This thermocouple was mounted on the tubular reactor in close contact with the catalyst bed to minimize the temperature difference between the catalyst bed and thermocouple. Another Type-K thermocouple was inserted in the middle of quartz tube to recheck possible temperature gradient; this inner-system thermocouple is covered with small closed-end quartz rod to prevent the catalytic reactivity of thermocouple during reaction. The recorded values showed that maximum temperature fluctuation during the reaction was always $\pm 1.0°C$ or less from the temperature specified for the reaction. It is noted that all experiments were carried out at isothermal condition after the system temperature was raised up to its setting temperature and waited until reaching steady state.

Catalysts (50 mg) were diluted with SiC (to obtain the total weight of 500 mg) to avoid temperature gradients and loaded in the quartz reactor. Preliminary experiments were carried out to find suitable conditions in which internal and external mass transfer effects are not predominant. Considering the effect of external mass transfer, based on the results from our previous publications,[27,28] the total flow rate was kept constant at 100 $cm^3\ min^{-1}$ under a constant residence time in all testing. The suitable average sizes of catalysts were also verified to confirm that the experiments were carried out without the effect of internal mass transfer limitation. After the reactions, the exit gas mixture was transferred via trace-heated lines to Porapak Q column Shimadzu 14B gas chromatograph (GC) and mass spectrometer (MS). The MS in which the sampling of exit gas was done by a quartz capillary and differential pumping was used for transient and carbon formation experiments, whereas the GC was applied to investigate steady-state condition experiments and to recheck the results from MS. It should be noted that, in this work, the reactivity was defined in terms of PFAD conversion and product distribution. PFAD conversion can be calculated based on the percent difference between PFAD in the feed and in the final product. Regarding the product distribution, the gaseous products from the reaction include H_2, CO, CO_2, CH_4, C_2H_6, C_2H_4, and C_3H_6; the yield of H_2 production (Y_{H_2}) was calculated by hydrogen balance defined as molar fraction of H_2 produced to total H_2 in the products. Other byproduct selectivities (i.e., S_{CO}, S_{CO_2}, S_{CH_4}, $S_{C_2H_6}$, $S_{C_2H_4}$, and $S_{C_3H_6}$) were calculated by carbon balance, defined as ratios of each product mole to the consumed moles of hydrocarbon, accounting for stoichiometry; this information was presented in terms of (relative) fraction of these byproduct components, which are summed to 100%.

Measurement of carbon formation

To investigate the amount of carbon formed on catalyst surface, the oxidation reaction was carried out by introducing 10% O_2 in He (with the flow rate of 100 $cm^3\ min^{-1}$) into the system at isothermal condition (1173 K), after being purged with He; the amount of carbon formation was determined by measuring the CO and CO_2 yields. The calibrations of CO and CO_2 productions were performed by injecting a known amount of these calibration gases from a loop in an injection valve in the bypass line. It is noted that the spent sample was further tested with TGA-MS (PerkinElmer, USA) at the maximum temperature of 1273 K to ensure that no carbon formation remains on the surface of catalyst, and no weight loss or CO/CO_2 productions were detected from all catalysts after oxidation reaction.

Results and Discussion

Reactivity of Ce-ZrO_2 toward partial oxidation of PFAD

The partial oxidation of PFAD over nanoscale Ce-ZrO_2 prepared by surfactant-assisted method (with Ce/Zr ratios of 1/3, 1/1, and 3/1) was first studied at 1123 K by feeding PFAD and O_2 with O/C molar ratio of 1.0. It can be seen in Figures 1a–c that, at this condition, H_2, CO, CH_4, and CO_2 are the main products with small amount of C_2H_4, C_2H_6, and C_3H_6 generated from the reaction. Furthermore, the conversions of PFAD and O_2 are always close to 100%, and small amount of water formation (<1%) is observed. For comparison, the homogeneous (noncatalytic) partial oxidation of PFAD was also investigated by feeding PFAD and O_2 with O/C molar ratio of 1.0 to the quartz tube filled with 500 mg of SiC at 1123 K. It was found that more than 90% of PFAD are converted; nevertheless, the main gaseous products formed are hydrocarbon compounds (i.e., CH_4, C_2H_4, C_2H_6, and C_3H_6 with the selectivities of 27.7, 23.3, 22.7, and 10.5%, respectively) with slight formations of CO and CO_2 (12.8% S_{CO} and 3.0% S_{CO_2}). Furthermore, significant amount of carbon was also detected in the blank reactor after exposure for 6 h.

The results from Figures 1a–c reveal that Ce-ZrO_2 with Ce/Zr ratio of 3/1 shows the best performance in terms of its high H_2 production with lowest C_2H_4, C_2H_6, and C_3H_6 formations. Furthermore, according to the postreaction oxidation experiment, the amount of carbon formation on the surface of Ce-ZrO_2 with Ce/Zr ratio of 3/1 after reaction (48 h) was relatively lower than other two ratios (3.4 mmol g_{cat}^{-1} compared with 4.3 and 4.7 mmol g_{cat}^{-1} observed over Ce-ZrO_2 with Ce/Zr ratios of 1/1 and 1/3, respectively). For comparison, the partial oxidation of PFAD over microscale Ce-ZrO_2 prepared by coprecipitation method (with Ce/Zr ratios of 1/3, 1/1, and 3/1) was also carried out at the same operating conditions (1123 K with O/C molar ratio of 1.0). As shown in Figure 2, less H_2 production with relatively higher C_2H_4, C_2H_6, and C_3H_6 formations was observed over this microscale Ce-ZrO_2. In addition, the postreaction oxidation also detected significantly higher amount of carbon formation over this catalyst (4.2, 4.9, and 5.6 mmol g_{cat}^{-1} over Ce-ZrO_2 with Ce/Zr ratios of 3/1, 1/1, and 1/3, respectively). These results strongly indicate the better reaction performance for nanoscale Ce-ZrO_2 (with Ce/Zr molar ratio of 3/1); hence, this catalyst was chosen for further studies and analyses.

The effect of inlet O_2 content on the catalytic reactivity was then studied by introducing PFAD and O_2 with O/C molar ratios of 0.5, 0.75, 1.0, 1.25, and 1.5 to the catalytic

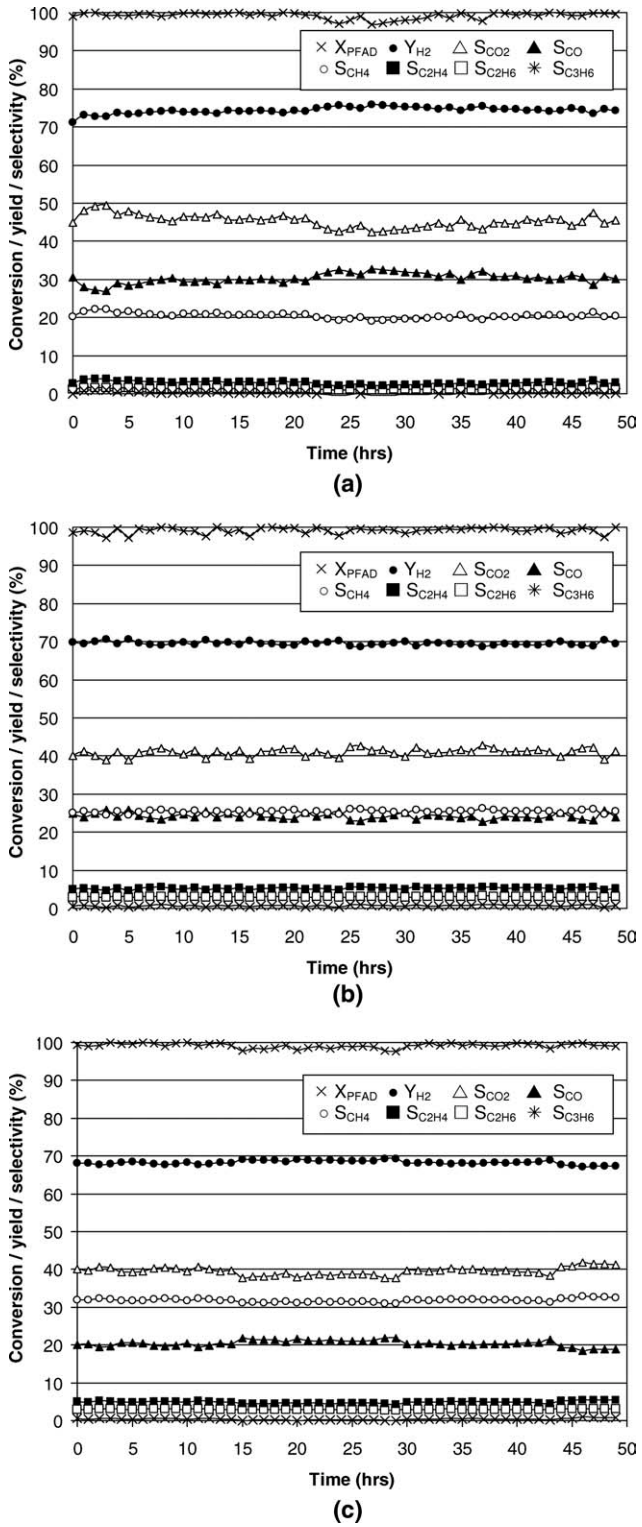

Figure 1. Reactivities of nanoscale Ce-ZrO_2 with various Ce/Zr molar ratios toward the partial oxidation of PFAD (at 1123 K with O/C molar ratio of 1.0).

The variations in conversion and product distributions with time from partial oxidation of PFAD over (a) Ce-ZrO_2 (Ce/Zr molar ratio of 3/1), (b) Ce-ZrO_2 (Ce/Zr molar ratio of 1/1), and (c) Ce-ZrO_2 (Ce/Zr molar ratio of 1/3).

reactor. At steady-state condition, H_2 production and the distribution of all gaseous byproducts (i.e., hydrocarbons, CO, and CO_2) were measured as shown in Figure 3. It can be seen that H_2 and CO increased with increasing O_2 content until inlet O/C ratio reached 1.25. On the contrary, these products decreased when the ratio was higher, whereas the distribution of CO_2 grew up. This is mainly due to the combustion of H_2 and CO by O_2 in the feed. With increasing O_2 content, the conversions of C_2H_4, C_2H_6, and C_3H_6 increased and reached 100% at O/C molar ratio of 1.25. For CH_4 formation, it increased when inlet O/C molar ratio changed from 0.5 to 1.25 but slightly decreased at higher O_2 content. These behaviors are related to the decompositions of C_2H_4, C_2H_6, and C_3H_6 to CH_4 at low inlet O_2 concentration and the further conversion of CH_4 to CO, CO_2, and H_2 at higher O_2 content. We previously reported the efficient decomposition of C_2H_6 and C_2H_4 to CH_4 in this range of temperature studied.[28]

It is noted that the effect of temperature on the conversion and product distribution was also carried out by varying the operating temperatures from 973 to 1173 K while keeping O/C molar ratio constant at 1.0. It was observed that H_2, CO, and CH_4 increased with increasing temperature, whereas CO_2, C_2H_6, and C_2H_4 considerably decreased, as shown in Figure 4. The decrease of CO_2 is due to the influence of reverse water–gas shift reaction ($CO_2 + H_2 \rightarrow CO + H_2O$), whereas the increases of CH_4, CO, and H_2 come from the decomposition and (partial) oxidation of C_2H_6 and C_2H_4 at higher temperature. Theoretically, the formations of gaseous hydrocarbon (i.e., CH_4, C_2H_4, C_2H_6, and C_3H_6) occur from the decomposition of PFAD (Eq. 1), whereas H_2, CO, and CO_2 are generated from both thermal decomposition and partial oxidation reactions (Eqs. 2–4). It should also be noted that, apart from thermal decomposition of PFAD, CH_4 can also be generated from methanation reactions (Eqs. 5 and 6).

Thermal decomposition of fatty acids

$$C_xH_yCOOH \rightarrow C_nH_mO_k + \text{coke} + \text{gases}(H_2, CO, CO_2, C_nH_m) \quad (1)$$

Partial oxidation of gaseous hydrocarbons and possible side reactions

$$2C_nH_m + nO_2 \rightarrow n2CO + 2mH_2 \quad (2)$$

$$2CO + O_2 \rightarrow 2CO_2 \quad (3)$$

$$2H_2 + O2 \rightarrow 2H_2O \quad (4)$$

$$n\text{CO} + 3n\text{H2} \rightarrow n\text{CH4} + n\text{H}_2\text{O} \quad (5)$$

$$n\text{CO}_2 + 4n\text{H}_2 \rightarrow n\text{CH}_4 + 2n\text{H}_2\text{O} \quad (6)$$

We suggested that the good partial oxidation reactivity of Ce-ZrO_2 is related to the OSC of this material because we previously reported that at moderate temperature, lattice oxygen (O_O^x) at ceria surface can oxidize gaseous hydrocarbons (e.g., CH_4).[27,28] In addition, the doping of CeO_2 with Zr has been observed to improve OSC as well as thermal stability of the material.[29–32] These benefits were associated with enhanced reducibility of cerium (IV) in Ce-ZrO_2 because of

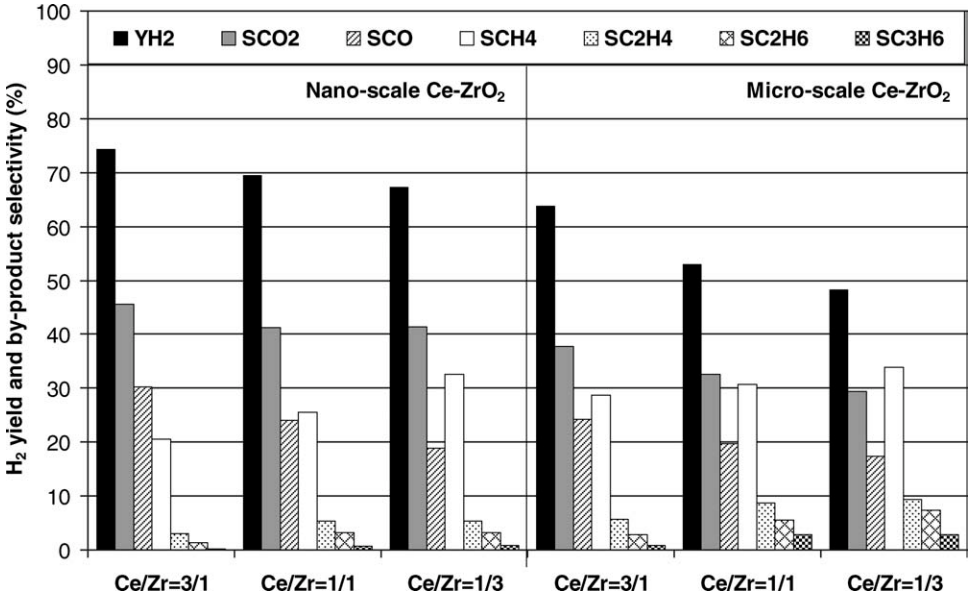

Figure 2. Reactivities of nanoscale and microscale Ce-ZrO_2 with various Ce/Zr molar ratios toward the partial oxidation of PFAD (at 1123 K with O/C molar ratio of 1.0).

The variations in product distributions from partial oxidation of PFAD at steady state (after 24 h) over nanoscale and microscale Ce-ZrO_2 with Ce/Zr molar ratios of 3/1, 1/1, and 1/3.

the high O^{2-} mobility inside the fluorite lattice.[26] During partial oxidation reaction, the gas–solid reactions between hydrocarbons present in the system (i.e., CH_4, C_2H_4, C_2H_6, and C_3H_6) and $O_O{}^x$ take place forming CO and H_2 from which the formation of carbon is thermodynamically unfavorable. The possible reaction pathway for partial oxidation of PFAD over Ce-ZrO_2 is illustrated below:

C_nH_m adsorption

$$CnHm + (n+m)^* \rightarrow (CH_x^*) + (H^*) \rightarrow n(C^*) + m(H^*) \quad (7)$$

Coreactant (O_2) adsorption

$$O_2 + 2^* \Leftrightarrow 2O^* \quad (8)$$

Redox reactions of lattice oxygen ($O_O{}^x$) with C* and O*

$$C^* + O_O^x \rightarrow CO^* + V_o^{\bullet\bullet} + 2e' \quad (9)$$

$$V_o^{\bullet\bullet} + 2e' + O^* \Leftrightarrow O_O{}^x + * \quad (10)$$

Desorption of products (CO and H_2)

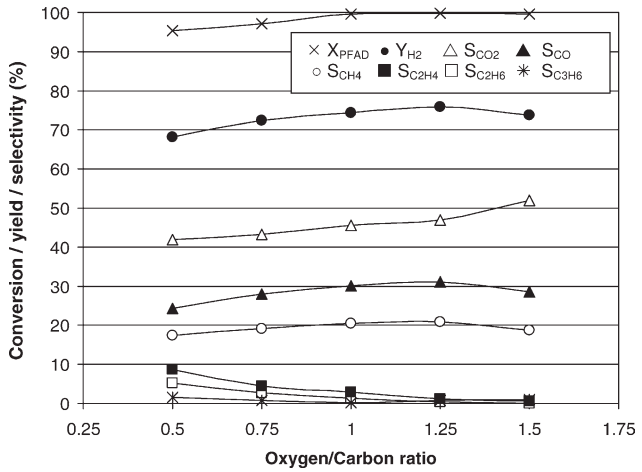

Figure 3. Partial oxidation of PFAD over nanoscale Ce-ZrO_2 (Ce/Zr molar ratio of 3/1) at various inlet O/C molar ratios.

Effect of inlet O/C molar ratio on the product compositions from the partial oxidation of PFAD over nanoscale Ce-ZrO_2 (Ce/Zr molar ratio of 3/1).

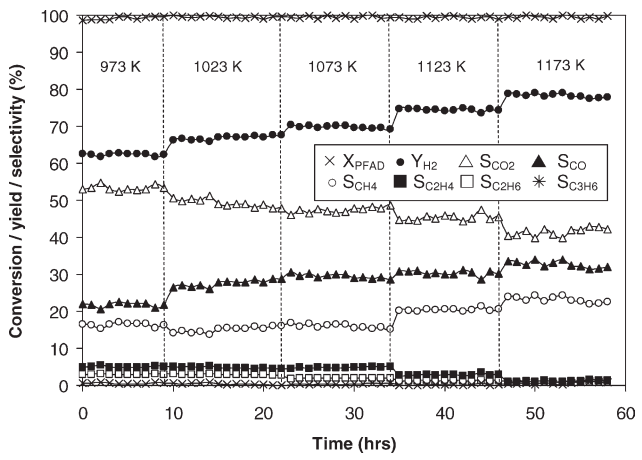

Figure 4. Product compositions from the partial oxidation of PFAD over nanoscale Ce-ZrO_2 (Ce/Zr molar ratio of 3/1) at various temperatures.

Effect of temperature on the product compositions from the partial oxidation of PFAD over nanoscale Ce-ZrO_2 (Ce/Zr molar ratio of 3/1).

Table 1. Effects of Temperature and Oxygen/Carbon Molar Ratio on the Degrees of Carbon Formation Over Ce-zrO_2 After Exposure to Partial Oxidation of PFAD

Catalyst	Temperature (K)	Oxygen/Carbon Molar Ratio	Carbon Formation (mmol g_{cal}^{-1})
Ce-ZrO_2 (Ce/Zr = 3/1)	1123	0.5	5.3 ± 0.15
	1123	0.75	4.2 ± 0.09
	1123	1.0	3.4 ± 0.10
	1123	1.25	2.9 ± 0.24
	1123	1.5	2.7 ± 0.17
	973	1.0	4.3 ± 0.11
	1023	1.0	3.9 ± 0.02
	1073	1.0	3.6 ± 0.15
	1173	1.0	3.0 ± 0.19

$$CO^* \Leftrightarrow CO + * \quad (11)$$

$$2(H^*) \Leftrightarrow H_2 + 2^* \quad (12)$$

Based on the Kroger–Vink notation, $V_O^{\bullet\bullet}$ denotes an oxygen vacancy with an effective charge 2^+, and e′ is an electron which can either be more or less localized on a cerium ion or delocalized in a conduction band. * is the surface active site of ceria-based materials. During the reaction, hydrocarbons adsorbed on * forming intermediate surface hydrocarbon species (CH_x* and eventually C* and H*) (Eq. 7). This C* later reacted with lattice oxygen ($O_O{}^x$) (Eq. 9). The steady-state rate is due to the continuous supply of oxygen source by inlet O_2 that reacted with the reduced-state catalyst to recover lattice oxygen ($O_O{}^x$) (Eqs. 8 and 10). It is noted that, according to our previous studies, * can be considered as unique site or same site as lattice oxygen ($O_O{}^x$).[27,28] During the reaction, hydrocarbons adsorbed on either unique site or lattice oxygen ($O_O{}^x$), whereas O_2 reacted with the catalyst reduced site to regenerate $O_O{}^x$ as well as remove the formation of carbon species on the catalyst surface. In this work, the amount of carbon formation (mmol g_{cat}^{-1}) on the surface of Ce-ZrO_2 after exposure to the partial oxidation at several inlet conditions (various O/C molar ratios and operating temperatures) was also determined, as reported in Table 1. Clearly, the carbon formation decreased with increasing temperature and oxygen content. Theoretically, the following reactions are the most probable reactions that could lead to carbon formation during the partial oxidation of PFAD

$$2CO \Leftrightarrow CO_2 + C \quad (13)$$

$$C_nH_m \Leftrightarrow 0.5mH_2 + nC \quad (14)$$

$$CO + H_2 \Leftrightarrow H_2O + C \quad (15)$$

$$CO_2 + 2H_2 \Leftrightarrow 2H_2O + C \quad (16)$$

At low temperature, reactions (15)–(16) are favorable, whereas reactions (13) and (14) are thermodynamically unfavored. The Boudouard reaction (Eq. 13) and the decomposition of hydrocarbons (Eq. 14) are the major pathways for carbon formation at such a high temperature as they show the largest decreased in Gibbs energy.[33,34] Based on the range of temperature in this study, carbon formation would be formed via the decomposition of hydrocarbons and Boudouard reactions especially at low inlet O/C molar ratio. By applying ceria-based catalysts, both reactions could be inhibited by the redox reaction between surface carbon (C) and lattice oxygen ($O_O{}^x$) (Eq. 9), whereas the oxygen vacancy is recovered via the reactions with supply of O_2 source (Eqs. 8 and 10).

Oxygen storage capacity and lattice oxygen mobility measurements

The higher reactivity with greater resistance toward carbon deposition for nanoscale Ce-ZrO_2 with Ce/Zr ratio of 3/1 compared with microscale Ce-ZrO_2 and Ce-ZrO_2 with Ce/Zr ratios of 1/1 and 1/3 could be due to the better redox properties (e.g., OSC) of this catalyst. To prove this explanation, the OSC of all Ce-ZrO_2 was determined by the isothermal reduction measurement (R-1), which was performed by purging the catalysts with 5% H_2 in He at 1173 K. The amount of H_2 uptake is correlated to the amount of O_2 stored in the catalysts. As presented in Figure 5 and Table 2, the amount of H_2 uptake over nanoscale Ce-ZrO_2 with Ce/Zr of 3/1 is significantly higher than other Ce-ZrO_2. The redox reversibilities of these catalysts were also determined by applying the oxidation measurement (Ox-1) followed by second-time reduction measurement (R-2) at the same conditions. The amounts of O_2 chemisorbed and H_2 uptakes (from both R-1 and R-2) are presented in Table 2. From these results, the amounts of H_2 uptake from R-2 were approximately identical to those from R-1, indicating the reversibility of OSC for these synthesized Ce-ZrO_2.

In addition to the OSC, the $^{18}O/^{16}O$ isotope exchange experiment was carried out to investigate the lattice oxygen mobility of these Ce-ZrO_2. The sample (200 mg) was placed in the quartz reactor and thermally treated under the flow of high-purity helium (99.995%) at the desired temperatures for 1 h. Then, $^{18}O_2$ (in helium as carrier gas) was multiple times pulsed to the system and the outlet gases were monitored by

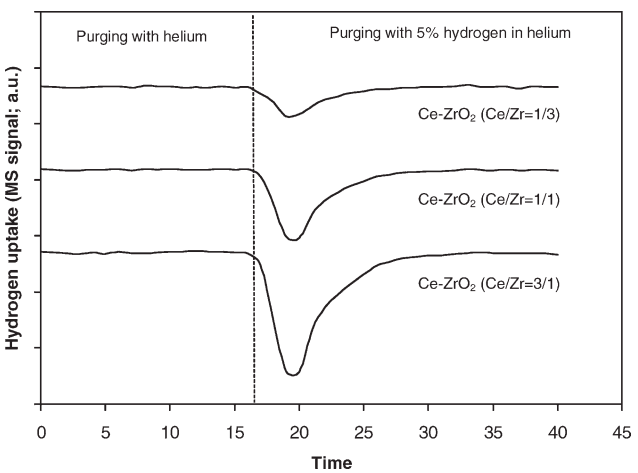

Figure 5. Oxygen storage capacity measurement of nanoscale Ce-ZrO_2 with various Ce/Zr molar ratios.

Isothermal reduction testing (at 1123 K) over nanoscale Ce-ZrO_2 with Ce/Zr molar ratios of 1/3, 1/1, and 3/1.

Table 2. Results of R-1, Ox-1, and R-2 Analyses of Nanoscale and Microscale Ce-ZrO_2 with Different Ce/Zr Ratios

Catalyst	H_2 Uptake from R-1 (μmol g_{cal}^{-1})	O_2 Uptake from Ox-1 (μmol g_{cal}^{-1})	H_2 Uptake from R-2 (μmol g_{cal}^{-1})
Nanoscale Ce-ZrO_2 (Ce/Zr = 1/3)	2883	1423	2879
Nanoscale Ce-ZrO_2 (Ce/Zr = 1/1)	3692	1848	3687
Nanoscale Ce-ZrO_2 (Ce/Zr = 3/1)	5221	2620	5213
Microscale Ce-ZrO_2 (Ce/Zr = 1/3)	1087	551	1075
Microscale Ce-ZrO_2 (Ce/Zr = 1/1)	1701	709	1694
Microscale Ce-ZrO_2 (Ce/Zr = 3/1)	2625	1305	2621

the MS. According to our results, the productions of $^{16}O_2$ and $^{18}O^{16}O$ for nanoscale Ce-ZrO_2 with Ce/Zr of 3/1 were 18 and 14% at 600°C, whereas those for nanoscale Ce-ZrO_2 with Ce/Zr of 1/1 and Ce-ZrO_2 with Ce/Zr of 1/3 were 13 and 6% (Ce/Zr of 1/1) and 9 and 2% (Ce/Zr of 1/3) at the same temperature. Thus, the higher oxygen mobility of Ce-ZrO_2 with Ce/Zr of 3/1 can be confirmed. As for the testing over microscale Ce-ZrO_2, the productions of $^{16}O_2$ and $^{18}O^{16}O$ at 600°C for this Ce-ZrO_2 with Ce/Zr of 3/1, 1/1, and 1/3 were 11 and 7%, 9 and 5%, and 6 and 2%, respectively.

It can be seen that the partial oxidation reactivity, the OSC, and the lattice oxygen mobility of Ce-ZrO_2 are in the same trend (nanoscale Ce-ZrO_2 < microscale Ce-ZrO_2; Ce-ZrO_2 with Ce/Zr of 3/1 > Ce-ZrO_2 with Ce/Zr of 1/1 > Ce-ZrO_2 with Ce/Zr of 1/3), indicating the strong impact of the catalyst specific surface area, the OSC, and the lattice oxygen mobility on the catalyst reactivity.

The application of Ce-ZrO_2 as preoxidative catalyst

From Section "reactivity of Ce-ZrO_2 toward partial oxidation of PFAD," the great benefit of partial oxidation over nanoscale Ce-ZrO_2 is its high resistance toward carbon deposition; nevertheless, the remaining detectable of hydrocarbons (i.e., CH_4, C_2H_4, C_2H_6, and C_3H_6) in the product indicates the incomplete conversion of PFAD by this catalyst. Therefore, we further studied the potential for applying Ce-ZrO_2 as preoxidative catalyst to initially convert PFAD to light products; the product gas from this primary partial oxidation part was then mixed with steam and simultaneously fed to the secondary steam reforming over Ni/Ce-ZrO_2 to complete the hydrocarbon conversion and maximize H_2 yield. In this experiment, the initial feed was PFAD and O_2 with O/C molar ratio of 1.25. At the exit of the partial oxidation reaction, the steam was then added with H_2O/C molar ratio of 3.0. It is noted that the carbon considered for this H_2O/C ratio is based on the amount of unconverted carbon compounds (i.e., CH_4, C_2H_4, C_2H_6, and C_3H_6) from the partial oxidation part. Figure 6 presents the H_2 yield and other gaseous products from this coupling system at various temperatures; it can be seen that H_2 production is significantly high, and the formations of hydrocarbons, i.e., CH_4, C_2H_4, and C_2H_6, are closed to 0 particularly at high operating temperature. It was also revealed that CO and H_2 increase with increasing temperature, whereas CO_2, C_2H_4, and C_2H_6 decrease. The dependence of CH_4 on the operating temperature was nonmonotonic, and the maximum production of CH_4 occurred at ~1073 K. The increase of CH_4 at low temperature comes from the decomposition of all hydrocarbons (PFAD, C_2H_4, and C_2H_6), whereas the decrease at higher temperature could be due to the further reforming to CO and H_2; the increase in H_2O conversion (from 41% at 1073 K to 45 and 48% at 1123 and 1173 K) strongly supports this explanation. It is noted according to the postreaction oxidation measurement that low carbon formation (in the range of 3.2–4.7 mmol g_{cat}^{-1}) was observed from the spent catalysts; moreover, the amount of carbon formation (as well as the percentage of CH_4 in the end product) can be further minimized by increasing the inlet steam content, as presented in Table 3 and Figure 7. For comparison, the steam reforming of PFAD over Ni/Ce-ZrO_2 (without preoxidation with Ce-ZrO_2) was also tested. Unstable profiles of H_2 production, which

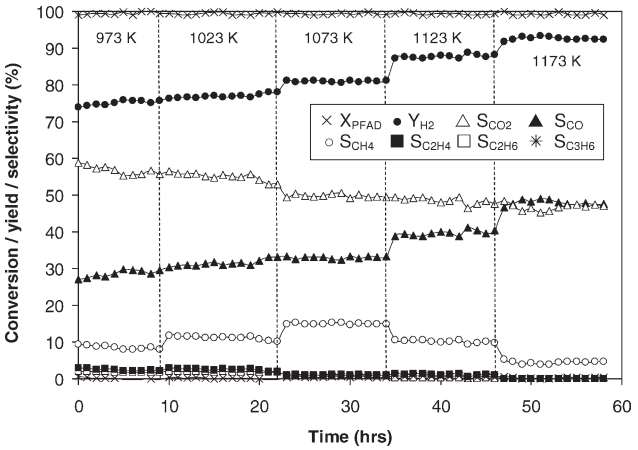

Figure 6. Preoxidation of PFAD with nanoscale Ce-ZrO_2 followed by the steam reforming over Ni/Ce-ZrO_2 at various temperatures.

Effect of temperature on the product compositions from the preoxidation of PFAD with nanoscale Ce-ZrO_2 followed by the steam reforming over Ni/Ce-ZrO_2.

Table 3. Effects of Temperature and Inlet Steam/Carbon Molar Ratio on the Degrees of Carbon Formation After Exposure to the Preoxidation of PFAD Over Ce-ZrO_2 (with O/C Molar Ratio of 1.25) Followed by the Steam Reforming Over Ni/Ce-ZrO_2

Catalyst	Temperature (K)	Steam/Carbon Molar Ratio	Carbon Formation (mmol g_{cat}^{-1})
Ce-ZrO_2 + Ni/Ce-ZrO_2	973	3.0	4.7 ± 0.29
	1023	3.0	4.4 ± 0.17
	1073	3.0	3.9 ± 0.11
	1123	3.0	3.6 ± 0.14
	1173	3.0	3.2 ± 0.06
	1173	5.0	3.1 ± 0.18
	1173	7.0	2.9 ± 0.10
	1173	9.0	2.7 ± 0.13
	1173	11.0	2.7 ± 0.07
	1173	13.0	2.6 ± 0.09

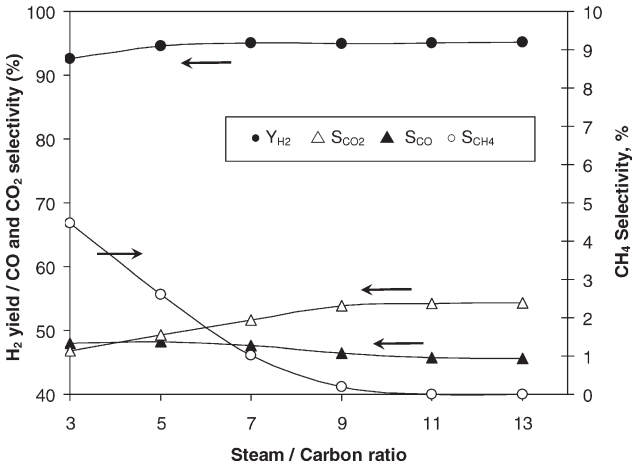

Figure 7. Preoxidation of PFAD with nanoscale Ce-ZrO_2 followed by the steam reforming over Ni/Ce-ZrO_2 at various inlet steam/carbon molar ratios.

Effect of inlet steam/carbon molar ratio on the product compositions from the preoxidation of PFAD with nanoscale Ce-ZrO_2 followed by the steam reforming over Ni/Ce-ZrO_2.

related to the high formation of carbon species on the surface of catalyst, were observed. After purging in He, the postreaction oxidation measurement detected significant amount of carbon over the catalyst (8.4 mmol g_{cat}^{-1}). This result indicates that Ni-based catalyst is inappropriate for the direct reform of PFAD and highlights the great benefit of nanoscale Ce-ZrO_2 as preoxidative catalyst.

Conclusions

Nanoscale Ce-ZrO_2 with Ce/Zr ratio of 3/1 has useful partial oxidation activity for converting PFAD (with almost 100% conversion) to H_2, CH_4, CO, and CO_2 with slight formations of gaseous high hydrocarbon compounds, i.e., C_2H_4, C_2H_6, and C_3H_6 under moderate temperature (1073–1173 K). The good reactivity was found to be closely related with the high OSC and lattice oxygen mobility of this synthesized catalyst, according to the reduction/oxidation measurement and $^{18}O/^{16}O$ isotope exchange study. It was also revealed that this nanoscale Ce-ZrO_2 can be efficiently used as the preoxidative catalyst to initially convert PFAD to light hydrocarbons, from which the latter reforms with steam in the presence of Ni-based catalyst to complete the hydrocarbon conversion and maximize H_2 yield.

Acknowledgment

The financial support from The Thailand Research Fund (TRF) throughout this project is gratefully acknowledged.

Literature Cited

1. Ahmed S, Krumpelt M. Hydrogen from hydrocarbon fuels for fuel cells. *Int J Hydrogen Energy*. 2001;26:291–301.
2. Seo YS, Shirley A, Kolaczkowski ST. Evaluation of thermodynamically favourable operating conditions for production of hydrogen in three different reforming technologies. *J Power Sources*. 2002;108:213–225.
3. Cheekatamarla PK, Finnerty CM. Synthesis gas production via catalytic partial oxidation reforming of liquid fuels. *Int J Hydrogen Energy*. 2008;33:5012–5019.
4. Wang H, Feldhoff A, Caro J, Schiestel T, Werth S. Oxygen selective ceramic hollow fiber membranes for partial oxidation of methane. *AIChE J*. 2009;55:2657–2664.
5. Tanaka H, Kaino R, Okumura K, Kizuka T, Tomishige K. Catalytic performance and characterization of Rh–CeO_2/MgO catalysts for the catalytic partial oxidation of methane at short contact time. *J Catal*. 2009;268:1–8.
6. Diehl F, Barbier J, Duprez D, Guibard I, Mabilon G. Catalytic oxidation of heavy hydrocarbons over Pt/Al_2O_3. Influence of the structure of the molecule on its reactivity. *Appl Catal B: Environ*. 2010;95:217–227.
7. Alvarez-Galvan MC, Navarro RM, Rosa F, Briceño Y, Gordillo Alvarez F, Fierro JLG. Performance of La,Ce-modified alumina-supported Pt and Ni catalysts for the oxidative reforming of diesel hydrocarbons. *Int J Hydrogen Energy*. 2008;33:652–663.
8. Shi L, Bayless DJ, Prudich ME. A CFD model of autothermal reforming. *Int J Hydrogen Energy*. 2009;34:7666–7675.
9. Recupero V, Pino L, Leonardo RD, Lagana M, Maggio G. Hydrogen generator, via catalytic partial oxidation of methane for fuel cells. *J Power Sources*. 1998;71:208–214.
10. Basagiannis AC, Verykios XE. Influence of the carrier on steam reforming of acetic acid over Ru-based catalysts. *Appl Catal B: Environ*. 2008;82:77–88.
11. Basagiannis AC, Verykios XE. Catalytic steam reforming of acetic acid for hydrogen production. *Int J Hydrogen Energy*. 2007;32:3343–3355.
12. Davidian T, Guilhaume N, Daniel C, Mirodatos C. Continuous hydrogen production by sequential catalytic cracking of acetic acid. I. Investigation of reaction conditions and application to two parallel reactors operated cyclically. *Appl Catal A: Gen*. 2008;335:64–73.
13. Liu N, Yuan Z, Wang C, Wang S, Zhang C, Wang S. The role of CeO_2–ZrO_2 as support in the ZnO–$ZnCr_2O_4$ catalysts for autothermal reforming of methanol. *Fuel Process Technol*. 2008;89:574–581.
14. Damyanova S, Pawelec B, Arishtirova K, Martinez Huerta MV, Fierro JLG. The effect of CeO_2 on the surface and catalytic properties of Pt/CeO_2–ZrO_2 catalysts for methane dry reforming. *Appl Catal B: Environ*. 2009;89:149–159.
15. Vagia EC, Lemonidou AA. Investigations on the properties of ceria–zirconia-supported Ni and Rh catalysts and their performance in acetic acid steam reforming. *J Catal*. 2010;269:388–396.
16. Chen J, Wu Q, Zhang J, Zhang J. Effect of preparation methods on structure and performance of Ni/Ce0.75Zr0.25O_2 catalysts for CH_4–CO_2 reforming. *Fuel*. 2008;87:2901–2907.
17. Cao L, Pan L, Ni C, Yuan Z, Wang S. Autothermal reforming of methane over Rh/Ce0.5Zr0.5O_2 catalyst: effects of the crystal structure of the supports. *Fuel Process Technol*. 2010;91:306–312.
18. Yuan Z, Ni C, Zhang C, Gao D, Wang S, Xie Y, Okada A. Rh/MgO/Ce0.5Zr0.5O_2 supported catalyst for autothermal reforming of methane: the effects of ceria–zirconia doping. *Catal Today*. 2009;146:124–131.
19. Lima SM, Cruz IO, Jacobs G, Davis BH, Mattos LV, Noronha FB. Steam reforming, partial oxidation, and oxidative steam reforming of ethanol over Pt/$CeZrO_2$ catalyst. *J Catal*. 2008;257:356–368.
20. Ozawa M, Kimura M, Isogai A. The application of CeZr oxide solid solution to oxygen storage promoters in automotive catalysts. *J Alloys Compd*. 1993;193:73–75.
21. Balducci G, Kaspar J, Fornasiero P, Graziani M, Islam MS. Surface and reduction energetics of the CeO_2-ZrO_2 catalysts. *J Phys Chem B*. 1998;102:557–561.
22. Vlaic G, Fornasiero P, Geremia S, Kaspar J, Graziani M. Relationship between the zirconia-promoted reduction in the Rh-loaded Ce0.5Zr0.5O_2 mixed oxide and the Zr-O local structure. *J Catal*. 1997;168:386–392.
23. Rao GR, Kaspar J, Meriani S, Dimonte R, Graziani M. NO decomposition over partially reduced metallized CeO_2-ZrO_2 solid solutions. *Catal Lett*. 1994;24:107–112.
24. Fornasiero P, Dimonte R, Rao GR, Kaspar J, Meriani S, Trovarell A, Graziani M. Rh-loaded CeO_2-ZrO_2 solid-solutions as highly efficient oxygen exchangers: dependence of the reduction behavior and

the oxygen storage capacity on the structural-properties. *J Catal*. 1995;151:168–177.
25. Yao MH, Hoost TE, Baird RJ, Kunz FW. An XRD and TEM investigation of the structure of alumina-supported ceria-zirconia. *J Catal*. 1997;166:67–74.
26. Kim D. Lattice parameters, ionic conductivities, and solubility limits in fluorite-structure MO_2 oxide [M = Hf4+, Zr4+, Ce4+, Th4+, U4+] solid solutions. *J Am Ceram Soc*. 1989;72:1415–1421.
27. Laosiripojana N, Assabumrungrat S. Catalytic dry reforming of methane over high surface area ceria. *Appl Catal B: Environ*. 2005; 60:107–116.
28. Laosiripojana N, Assabumrungrat S. Kinetic dependencies and reaction pathways in hydrocarbon and oxyhydrocarbon conversions catalyzed by ceria-based materials. *Appl Catal B: Environ*. 2008; 82: 103–113.
29. Laosiripojana N, Chadwick D, Assabumrungrat S. Effect of high surface area CeO_2 and Ce-ZrO_2 supports over Ni catalyst on CH_4 reforming with H_2O in the presence of O_2, H_2, and CO_2. *Chem Eng J*. 2008;138:264–273.
30. Kruse N, Frennet A, Bastin JM, editors. *Catalysis and Automotive Pollution Control IV*. Amsterdam: Elsevier, 1998.
31. Kaspar J, Fornasiero P, Graziani M. Use of CeO_2-based oxides in the three-way catalysis. *Catal Today*. 1999;50:285–298.
32. Roh HS, Potdar HS, Jun KW. Carbon dioxide reforming of methane over co-precipitated Ni-CeO_2, Ni-ZrO_2 and Ni-Ce-ZrO_2 catalysts. *Catal Today*. 2004;93–95:39–44.
33. Lwin Y, Daud WRW, Mohamad AB, Yaakob Z. Hydrogen production from steam–methanol reforming: thermodynamic analysis. *Int J Hydrogen Energy*. 2000;25:47–53.
34. Amor JN. The multiple roles for catalysis in the production of H_2. *Appl Catal A: Gen*. 1999;176:159–176.

Manuscript received May 12, 2010, revision received Sep. 7, 2010, and final revision received Oct. 29, 2010.